XVIII IMEKO WORLD CONGRESS
Metrology for a Sustainable Development
September, 17 – 22, 2006, Rio de Janeiro, Brazil

THERMAL Σ-Δ MODULATOR: PERFORMANCE ANALYSIS

L. S. Palma[1], *A. Oliveira*[1], *R. C. S. Freire*[2], *A. B. Fontes*[1]

[1] Federal University of Bahia, Salvador, Brazil, ligia@ufba.br, amauri@ufba.br, adhemar@ufba.br
[2] Federal University of Campina Grande, Campina Grande, Brazil, freire@dee.ufcg.edu.br

Abstract: This work presents the system performance analysis, in terms of frequency response and system resolution, of a 1-bit first-order Σ-Δ thermal modulator. In this system model, some of the operations conversion is performed by the thermoresistive sensor, which operates at constant temperature method. The system performance analysis was realized with a sampled version of the continuous time thermal Σ-Δ modulator. It will be shown that system performance is dependent on the system oversampling ratio (OSR) and the system transfer function pole and zero which depends on thermal and physical sensor characteristics and system operation conditions. This system was proposed as a solar radiation meter, but it may be applied to fluid velocity measurement.

Keywords: transducer, thermal Σ-Δ modulation, frequency response, thermoresistive sensor.

1. INTRODUCTION

In the classical architectures of solar radiation meters based on the equivalence principle and in which the sensing element is a thermoresistive sensor, the estimated output signal is in analog form [1]. The analog output may be treated with analog filter or can be converted to digital format by using an ADC at Nyquist rate. In both cases the system architecture demands complex circuitry. Even in the architecture which output signal is in digital format it needs to use ADC at Nyquist rate sampling to convert reference system value [2-3]. In this case, the resolution depends on ADC at Nyquist rate sampling bit number, which also demands complex circuitry when we think about microsensors.

A 1-bit first-order thermal Σ-Δ modulation, which includes a thermoresistive sensor in modulation loop, was proposed as solar radiation meter. It is based on equivalence principle and sensor constant temperature operation method [4]. This system gives solar radiation estimation, in digital format, directly from physical signal and may be integrated with a microsensor.

In the proposed modulator architecture the sensor substituted the sum and integration operations of the original 1-bit first-order Σ-Δ modulator [5] and this fact turns the purposed architecture into a thermal Σ-Δ modulator version. Our previous paper discussed operation function principle but not system performance. Now we discuss this item. To do this, we develop a sampled time version of the continuous signal system to extract performance parameters.

2. PURPOSE

Our system model, in which the sensor substitutes the original 1-bit first-order Σ-Δ modulator sum and integration operations, can be seen in fig. 1. This is a continuous signal architecture, which was used to study system behaviour. Another system architecture very close to the version to be implemented is the pulsed current system version and can be seen in fig. 2. In those models, the sensor resistance variation due to the sensor temperature variation was modelled by equation of a positive temperature coefficient thermoresistive sensor and is expressed by Eq. (1):

$$R_s(t) = R_0(1 + \beta T_s(t)) \tag{1}$$

R_0 is the sensor resistance at $0\ ^oC$ and β is the thermal coefficient which is a function of the sensor material.

The sensor thermodynamic behaviour is modelled by Eq. (2):

$$mc\frac{dT_s(t)}{dt} = hS(T_a(t) - T_s(t)) + R_s(t)I_s^2(t) + \alpha SH(t) \tag{2}$$

In this equation αSH is the incident thermal radiation captured by sensor, $I_s^2R_s = Y_sR_s$ is the electrical power delivered to the sensor, h is the heat transfer coefficient referred to the sensor surface area S, T_s is the sensor temperature, T_a is the surrounding temperature (ambient or fluid temperature), m is the sensor mass and c is the sensor specific heat. The system is project to operate at a constant temperature T_{s0}.

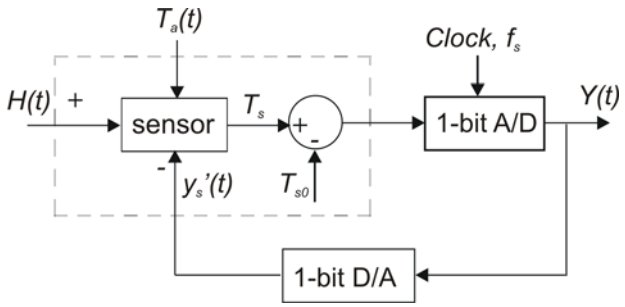

Fig. 1. Proposed architecture block diagram for continuous signal version.

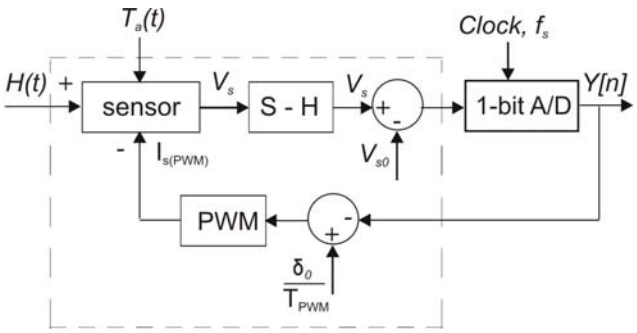

Fig.2. Proposed architecture block diagram for pulsed current system version.

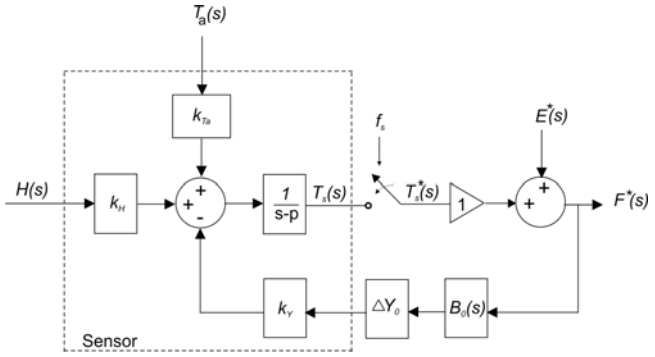

Fig. 3. System block diagram used to performance analysis.

As the sensor is projected to operate at constant temperature, a comparator is included into feedback loop to verify sensor temperature. If sensor temperature is greater than reference temperature, the quantizer generates a train of bits "1" at modulator output. These bits "1", introduced in modulator feedback path, reduce the sensor current that reduces the sensor temperature. If sensor temperature is less that reference temperature, the quantizer generates a train of bits "-1" at modulator output. These bits "-1" introduced in modulator feedback path increase the sensor current that increases the sensor temperature. This is the system control mechanism.

Our purpose is to verify the resolution that could be obtained with these architectures.

3. PERFORMANCE ANALYSIS

To analyze system performance, we develop a sampled version in *s*-domain of the proposed architecture that can be seen in fig. 3. The sensor was substituted by its small signal model, which was obtained for small signals variation near theoretical operation point. The sensor small signal model is described by Eq. (3).

$$T_s = \frac{1}{s-p}\left[k_{Ta}T_a(s) + k_H H(s) + k_Y Y_s(s)\right] \tag{3}$$

In which, p is the inverse of the sensor time constant, k_{Ta}, k_H and k_Y are the coefficients associated to environment temperature T_a, solar radiation H and sensor square current Y_s, respectively.

Figure 3 shows the sampled time version of the continuous signal system to extract performance parameters. The quantizer was linearized and modelled by a white noise source, $E^*(s)$, [6]-[7] and was added to the sensor temperature $T_s(s)$ which is a function of the solar radiation signal $H(s)$, and the surrounding temperature $T_a(s)$. $T_a(s)$ was compensated during simulation to the system correct operation. The unity gain block between sensor output and the white noise source has $°C^{-1}$ dimension, and realizes scale transformation from sensor temperature scale to the quantizer scale. A zero order hold, $B_0(s)$ in modulator feedback path, transforms modulator output samples to continuous signal. $B_0(s)$ is given by Eq. (4) with T been the oversampling period.

$$B_0(s) = \frac{1-e^{-sT}}{s} \tag{4}$$

3.1. System transfer function

The step response of H and T_a, for the 1-bit first-order Σ-Δ modulator with thermoresistive sensor is expressed by the transfer function in *z*-domain by Eq. (5).

$$F(z) = \left(\frac{z-r}{z-q}\right)E(z) - \left(\frac{k_{Ta}(1-r)}{p}\right)\left(\frac{1}{z-q}\right)T_a(z) - \\ -\left(\frac{k_H(1-r)}{p}\right)\left(\frac{1}{z-q}\right)H(z) \tag{5}$$

In which, r is the quantizer error transfer function zero and p is the system transfer function pole.

Solar radiation and surrounding temperature transfer functions had negative gains that provide attenuation to theses signals since the sensor must work at an almost constant temperature previously defined in system project.

The quantizer error transfer function (NTF) has a zero that depends on the sensor small signal model pole p, for $r = e^{pT}$ with T being the oversampling period. The system transfer function pole q also depends on this parameter, for $q = \frac{k_Y \Delta Y_0}{p}(1-r) + r$.

The NTF zero degrades the NTF noise attenuation in the signal band once there is a finite attenuation at DC frequency instead of an infinite attenuation as in ideal first-order sigma-delta modulator [6]-[7]. This may affect system resolution considerably.

3.2. Spectrum magnitude

The system NTF was manipulated to obtain its magnitude spectrum, which is expressed by Eq. (6).

$$E_y(f) = E(f)\frac{\sqrt{(1-r)^2 + 4r\sin^2\left(\frac{wT}{2}\right)}}{\sqrt{(1-q)^2 + 4r\sin^2\left(\frac{wT}{2}\right)}} \tag{6}$$

3.3. In-band noise power

The in-band noise power σ_{ey}^2, at the output of the converter was obtained assuming modulator output samples passing through an ideal low-pass filter with cut-off frequency f_B. The in-band noise power is given by Eq. (7). The in-band noise power depends on the OSR^{-1} and the quadratic relationship involving the NTF zero and pole.

$$\sigma_{ey}^2 = \int_{-f_B}^{f_B} \left|E_y(f)\right|^2 df = \sigma_{rms}^2 \left(\frac{2f_B}{f_s}\right)\left(\frac{(1-r)}{(1-q)}\right)^2 \quad (7)$$

3.4. Resolution

To obtain system theoretical resolution, system noise power was compared with *N*-bits Nyquist PCM noise power and the resolution, in bit number, is given by Eq. (8). This expression shows the resolution dependence with OSR^{-1} and and the quadratic relationship involving the NTF zero and pole.

$$N = -\frac{1}{2}\log_2\left[\left(\frac{1}{OSR}\right)\left(\frac{1-r}{1-q}\right)^2\right] \quad (8)$$

4. RESULTS

The sensor characteristics used in theoretical analysis and in system simulations were: $\beta=0{,}00385\ ^oC^{-1}$, $R_0=102{,}48\ \Omega$, $\alpha S=19x10^{-6}\ m^2$, $hS=2.982x10^{-3}\ W/^oC$, $mc=43{,}06x10^{-3}\ J/^oC$. The sensor temperature theoretical operation point was defined at 50 ^oC. To measure solar radiation in South America, the solar radiation scale was defined beginning from $H_{min}=0\ W/m^2$ and ending at $H_{max}=1600\ W/m^2$. Signal band frequency limit was chosen near system transfer function pole frequency, $f_B=0.9f_{sr}$.

Figure 4 shows theoretical system noise transfer function magnitude for oversamplig ratio equal to 256, zooming to signal in-band frequency. At DC there is a finite attenuation (-16.9 dB). This attenuation is degrading to –13.9 dB at NTF zero frequency and to –3 dB at NTF pole frequency. This fact puts an application limit to in-band frequency.

To obtain better system resolution the signal band must stay under system NTF zero frequency. The system NTF zero, in *s*-domain, is equal to sensor small signal transfer function pole. The maximum signal band frequency, in radians, must be less than the sensor small signal pole.

Figure 5 shows the system NTF zero and pole locations in *z*-plane. In this figure, it can be shown how close those two parameters are.

Figure 6 shows theoretical system resolution obtained by using Eq. (8) as an OSR function. The system resolution is improved by half bit every doubling of the oversampling ratio.

To verify theoretical results, the continuous signal current system and the pulsed current system were simulated in time domain for a sine wave input of solar radiation expressed by Eq. (9) to cover the full scale. The sine wave frequency was selected below sensor small model pole. The frequency used was *f=1/600 Hz*.

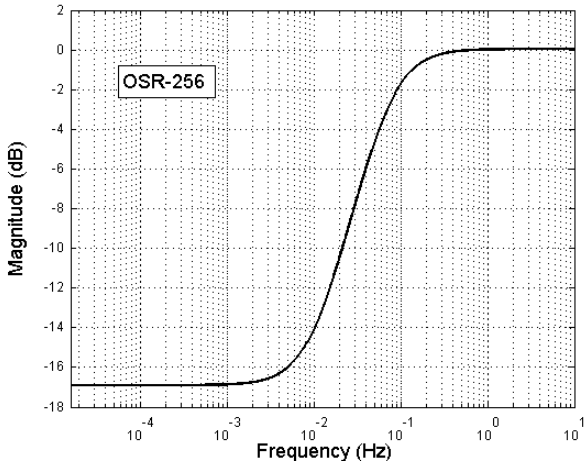

Fig. 4. System noise transfer function magnitude

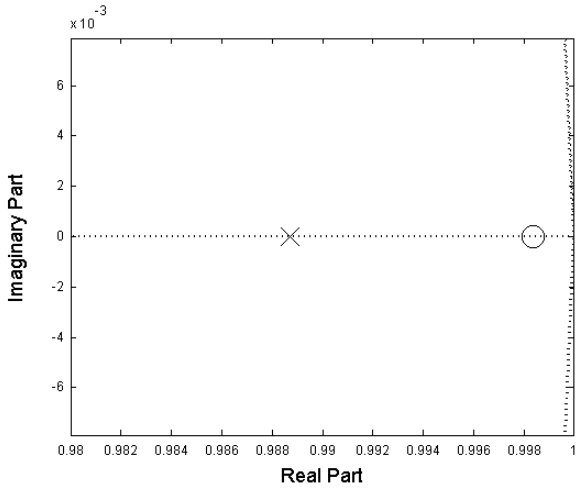

Fig. 5. System NTF zero-pole located in z-plane.

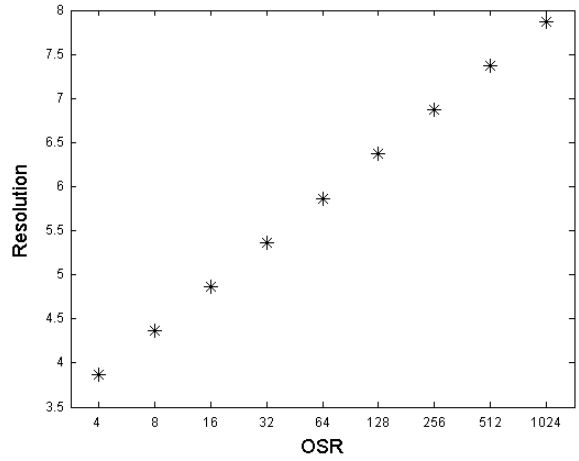

Fig. 6. System resolution.

$$H = 800 - 800\sin(2\pi ft)\ \ \mathrm{W/m^2} \quad (9)$$

Estimated solar radiation was obtained by simulation, after the samples *y[n]*, at the 1-bit first-order Σ-Δ modulator with thermoresistive sensor output, have moved through a

digital filter as presented in [8]. The surrounding temperature input signal was mathematically compensated.

Figure 7 and fig. 8 show estimated solar radiation absolute error for continuous signal system and pulsed current system, respectively. When considering solar radiation full scale of 1600 W/m^2 and not considering dynamic resolution lost located around positive peak of estimated solar radiation signal due to surrounding temperature compensation mathematical process these absolute errors are less than 15 W/m^2, less than 10 W/m^2 and less than 5 W/m^2 for OSR equal to 64, 128 and 256 respectively in both systems. The dynamic resolution lost, when taking in account, affects system resolution evaluation.

The medium square error in both systems was obtained from estimated solar radiation samples at the end of the converter after stabilization process and were calculated by Eq. (10):

$$\sigma_{ey}^2 = \left(\frac{2}{H_{\max} - H_{\min}} \right)^2 \frac{1}{N_a} \sum_{i=1}^{N_a} \left[H_n(i) - H(i) \right]^2 \qquad (10)$$

In which N_a is the number of samples, H_n is the estimated solar radiation at the output of the converter and H is the solar radiation at the input of the converter.

The estimated solar radiation square medium error was compared with N-bits Nyquist PCM noise power to obtain system resolution in time domain. The system resolution was given by Eq. (11):

$$N = -\frac{1}{2} \log_2 \left\{ \left(\frac{12}{(H_{\max} - H_{\min})^2} \right) \frac{1}{N_a} \sum_{i=1}^{N_a} \left[H_n(i) - H(i) \right]^2 \right\} \qquad (11)$$

Table 1 shows system resolution results obtained for three oversampling ratio values. The first column refers to system resolution results calculated by Eq. (8). The two and three columns refer to the continuous signal system and the pulsed current system time domain simulation results, respectively. They were calculated by Eq. (11). Continuous signal system absolute error leads to better results than pulsed current system absolute error. The problem is that the energy is not continuous in pulsed current system and represents a continuous signal system approximation. In these calculations we consider all samples, including those samples around estimated solar radiation signal positive peak (i.e., with dynamic resolution lost due to temperature compensation mathematical process).

5. CONCLUSION

The proposed 1-bit first-order thermal ∑−Δ modulator, when applied to physical greatness measurement like solar radiation measurement, leads to some operation limitations. The sensor small signal time constant or sensor small signal transfer function pole contributes to decrease quantization error attenuation at DC frequency affecting C. S. and P. C. systems resolution.

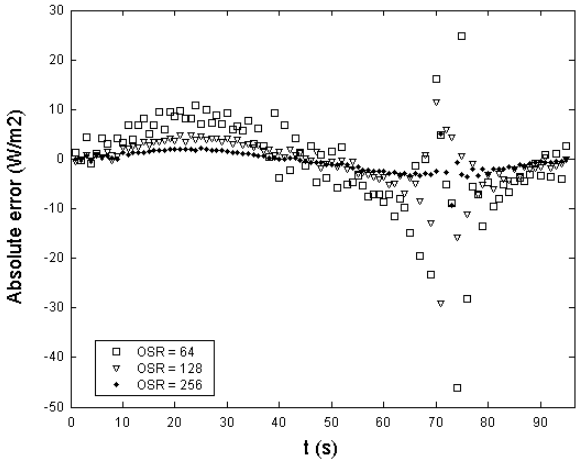

Fig. 7. Continuous signal system: estimated absolute error.

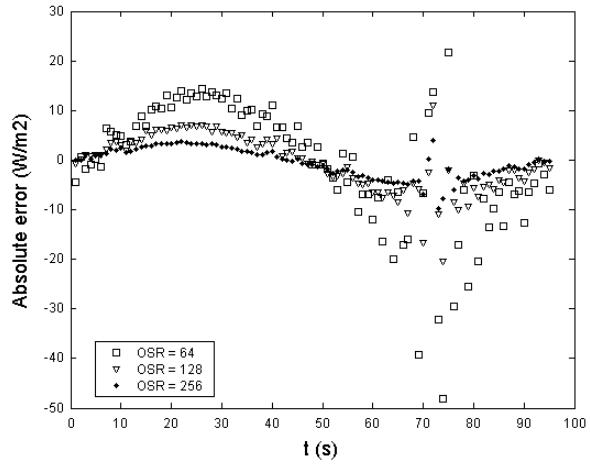

Fig. 8. Pulsed current system: estimated absolute error.

Table 1. Continuous current system and pulsed current system simulated resolution results.

	Resolution (bit number)		
OSR	**Theoretical System**	**Signal Current System**	**PWM System**
64	5.9	5.6	5.1
128	6.4	6.5	6.3
256	6.9	7.8	7.2

When comparing to ideal 1-bit ∑−Δ modulator, which is 1,5 bits for every doubling of the oversampling ratio, the resolution shown at Table 1 was worst.

To obtain better resolution operation condition, excitation signal band frequency must be limited under sensor small signal transfer function pole frequency and the modulator output samples must be filtered at the sensor small signal pole frequency.

ACKNOWLEDGMENTS

The authors wish to thank CAPES/Procad and CNPq for financial support and the award of fellowships during investigation period.

REFERENCES

[1] P. C. Lobo, R. C. S. Freire, G. S. Deep, J. S. Rocha Neto, A. M. N. Lima, "Dynamic Response of an Electronic Feedback Thermoresistive Substitution Pyranometer", Solar Engineering, vol 2, ASME, pp.751-756, 1995.

[2] A. Oliveira, G. S. Deep, A. M. N. Lima and R. C. S. Freire, "A Feedback I^2-Controlled Constant Temperature Solar Radiation Meter". IEEE Transactions on Instrumentation and Measurement, vol. 47, nº 5, pp.1062-1066, May 1998.

[3] L. S. Palma, A. Oliveira, A. S. Costa, A. Q. Andrade Jr, C. V. R. Almeida, M. E. P. V. Zurita and R. C. S. Freire, "Implementation of a Feedback I2-Controlled Constant Temperature Environment Temperature Meter", Sensors, vol. 3, issue 10, pp. 498-503, ISSN 1424-8220, 2003, http://www.mdpi.net/sensors.

[4] A. Oliveira, L. S. Palma, A. S. Costa, R. C. S. Freire, A. C. C. Lima, " A Constant Temperature Operation Thermoresistive Sigma-Delta Solar Radiometer", 10th IMEKO TC7 International Symposium on Advances of Measurement Science, vol. 1, pp 199-204, June 2004.

[5] H. Inose and Y. Yasuda, "A Unity Bit Coding Method by Negative Feedback", IEEE Procs., vol. 51, no 11, pp. 1524-1535, November 1963.

[6] P. M. Aziz, H. V. Sorensen and J. V. D. Spiegel, "An Overview of Sigma-Delta Converters", IEEE Signal Processing Magazine, pp. 61-84, January 1996.

[7] J. C. Candy and G. C. Temes, "Oversampling Methods for A/D and D/A Conversion". Oversampling Delta-Sigma Data Converters: Theory, Design and Simulation, IEEE Press, pp 1-25, 1992.

[8] S. Park, "Principles of Sigma-Delta Modulation for Analog-to-Digital Converters". Motorola DSP: Strategic Applications and Digital Signal Processor Operation, Motorola, 1998.